Standing Waves in a Two-Dimensional Reaction−Diffusion Model with the Short-Wave Instability

Milos Dolnik, Arkady B. Rovinsky, Anatol M. Zhabotinsky,* and Irving R. Epstein*

Department of Chemistry and Volen Center for Complex Systems, Brandeis University, Waltham, Massachusetts 02454-9110

Received: June 25, 1998; In Final Form: October 19, 1998

Various patterns of standing waves are found beyond the onset of the short-wave instability in a model reaction−diffusion system. These include plain and modulated stripes, squares, and rhombi in systems with square and rectangular geometry and patterns with rotational symmetry in systems with circular geometry. We also find standing waves consisting of periodic time sequences of stripes and rhombi, stripes and squares, and stripes, rhombi, and hexagons. The short-wave instability can lead to a much greater variety of spatio-temporal patterns than the aperiodic Turing and the long-wave oscillatory instabilities. For instance, a single oscillatory cycle can display all the basic patterns related to the aperiodic Turing instability—stripes, hexagons, and inverted hexagons (honeycomb)—as well as rhombi and modulated stripes.

I. Introduction

Wave patterns that arise from the oscillatory instability with finite wavelength (short-wave instability) have been much less thoroughly studied than those arising from the aperiodic Turing or the long wave oscillatory instability.[1,2] We have shown recently that the short-wave instability may be a source of a great variety of spatio-temporal patterns in one-dimensional media. These patterns include pure and modulated traveling and standing waves, alternating waves, asymmetric standing−traveling wave patterns and target patterns.[3−5] Here we expand our investigations to two-dimensional systems. As a guide to the patterns that may be expected, one can consider both the one-dimensional patterns arising from the wave instability and the two-dimensional patterns associated with the aperiodic Turing instability. In the latter case, the basic patterns are known to be hexagons and stripes.[2] In this paper, our primary goal is to study various types of standing waves at low degrees of supercriticality.

II. Model

We have developed a three-variable reaction−diffusion model that exhibits the wave instability.[3] The model is based on the following reaction scheme:

$$\mathrm{X} + 2\mathrm{Y} \rightarrow 3\mathrm{Y} \quad \text{(R1)}$$

$$\mathrm{S}_1 + 2\mathrm{Z} \rightarrow \mathrm{X} + 2\mathrm{Z} \quad \text{(R2)}$$

$$\mathrm{Y} \rightarrow \mathrm{P}_1 \quad \text{(R3)}$$

$$\mathrm{S}_2 + \mathrm{X} \rightarrow \mathrm{X} + \mathrm{Z} \quad \text{(R4)}$$

$$\mathrm{Z} \rightarrow \mathrm{P}_2 \quad \text{(R5)}$$

$$\mathrm{X} + \mathrm{C} \rightleftarrows \mathrm{XC} \rightarrow \mathrm{C} + \mathrm{P}_3 \quad \text{(R6)}$$

$$\mathrm{S}_3 \rightarrow \mathrm{Y} \quad \text{(R7)}$$

Here S_i are the initial reagents; P_j are the final products; and X, Y and Z are the intermediates, whose concentrations are the dynamic variables. C is a catalyst, and XC is the catalytic complex, whose reactions (R6) are assumed to be governed by Michaelis−Menten kinetics. The autocatalytic reaction (R1) is a principal source of instability in a variety of reaction schemes.[6] The wave instability results from the additional feedback loop: Z is the catalyst for X formation (R2), while X is the catalyst for Z formation (R4). The simpler scheme (R1)−(R5) generates the wave instability in the corresponding reaction−diffusion system; however, a much larger domain of the wave instability can be obtained with the additional reactions (R6) and (R7).[3]

The reaction−diffusion model in its dimensionless form corresponding to reaction scheme (R1)−(R7) is

$$\frac{\partial x}{\partial t} = m\left(-xy^2 + z^2 - \frac{ax}{g+x}\right) + d_x\Delta x$$

$$\frac{\partial y}{\partial t} = n(xy^2 - y + b) + d_y\Delta y \qquad (1)$$

$$\frac{\partial z}{\partial t} = x - z + \Delta z$$

where Δ is the Laplacian operator and

$$X = x_0 x, \quad Y = y_0 y, \quad Z = z_0 z, \quad t = k_5 t', \quad \xi_i = \left(\frac{k_5}{D_z}\right)^{0.5} x_i$$

$$x_0{}^3 = \frac{k_3{}^2 k_5{}^2}{k_1 k_2 k_4{}^2 S_1 S_2{}^2}, \quad y_0 = \frac{k_3}{k_1 x_0}, \quad z_0 = \frac{k_4 S_2}{k_5} x_0,$$

$$d_x = \frac{D_x}{D_z}, \quad d_y = \frac{D_y}{D_z} \qquad (2)$$

$$m = \frac{k_3 y_0}{k_5 x_0}, \quad n = \frac{k_3}{k_5}, \quad a = \frac{k_6 C}{k_3 y_0}, \quad b = \frac{k_7 S_3}{k_3 y_0}, \quad g = \frac{K_\mathrm{m}}{x_0}$$

K_m is the Michaelis constant of reaction (R6), and the concentrations of species other than X, Y, and Z are taken to be constant.

In the simulations presented here we set $D_x = D_y = 0$, which gives the largest domain of the wave instability. The value m_c

10.1021/jp982771j CCC: $18.00
Published on Web 12/10/1998

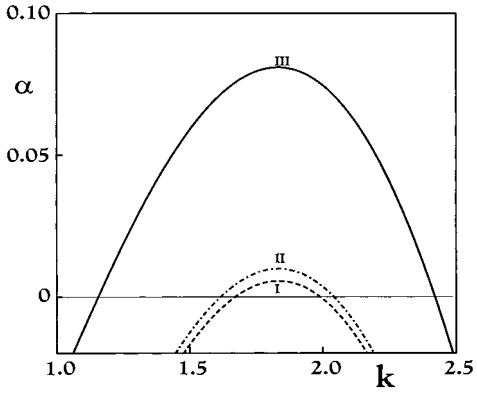

Figure 1. Dispersion curves at low degree of supercriticality in the vicinity of the short-wave bifurcation. Curve: (**I**) $m = 28.53$; (**II**) $m = 28.50$; (**III**) $m = 28.00$.

≈ 28.56915 corresponds to the short-wave bifurcation and $m_h \approx 26.79767$ to the spatially independent Hopf bifurcation.[3] The domain of pure short-wave instability is found for $m_h < m < m_c$. We refer to $\epsilon = (m_c - m)/m_c$ as the degree of supercriticality. The maximum of the dispersion curve (see Figure 1), occurs at a wavelength of approximately 3.426 space units. We refer to this value as the intrinsic wavelength in what follows. The intrinsic wavelength is nearly independent of m in the domain of pure short-wave instability.

In our simulations we keep constant the following parameters: $g = 1 \times 10^{-4}$, $a = 0.9$, $b = 0.2$, $n = 15.5$, and we vary the parameter m and size of the system.

Boundary and Initial Conditions. All simulations are done with zero flux boundary conditions.

In the majority of our simulations, we employ as initial conditions (IC) the homogeneous steady state with random uncorrelated deviations added to the x variable at each point of the two-dimensional grid. The random deviations are uniformly distributed on the interval ± 0.2 (18% of the steady-state value of x).

In some simulations, we employ regular patterns of local perturbations that correspond to the expected patterns of standing waves. In a few cases, we use the stationary patterns obtained from previous simulations as our IC in order to investigate the stability of the pattern at different values of the degree of supercriticality.

III. Numerical Procedure

The reaction−diffusion system (eq 1) was converted to a system of ordinary differential equations (ODE) by the method of lines (central difference spatial discretization with a uniform mesh). The resulting large ODE system was integrated with the stiff solver CVODE utilizing the sparse matrix linear equation solver.[7] Zero flux boundary conditions were used in all simulations. The grid size ranged from 80×80 to 400×400 grid points. We checked for spurious results of discretization by varying the spatial resolution of the grid. The number of grid points per intrinsic wavelength was always at least 10. The error tolerance of the CVODE solver was set to 1×10^{-6}. A fast Fourier transform (FFT)[8] was used to obtain two-dimensional Fourier power spectra of the patterns. Since the FFT requires a grid with 2^n nodes, the calculated patterns were linearly interpolated to the next largest power of two grids. For rectangular and square systems, eq 1 was represented in Cartesian coordinates, while polar coordinates were used for circular systems. In the latter case, the central point of the circle was still represented in Cartesian coordinates to avoid a numerical singularity.

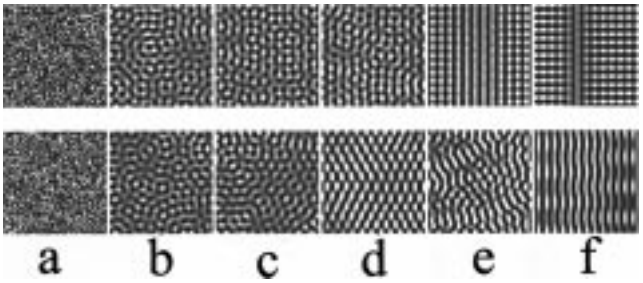

Figure 2. Development of standing waves from random initial conditions. Size of system 40×40 space units, $m = 28.5$. Values of x are quantified with 256 gray levels: white corresponds to the maximum value of x, black to the minimum value. Time (in dimensionless time units): 0 (a); 1000 (b); 2000 (c); 3000 (d); 4000 (e); 15 000 (f).

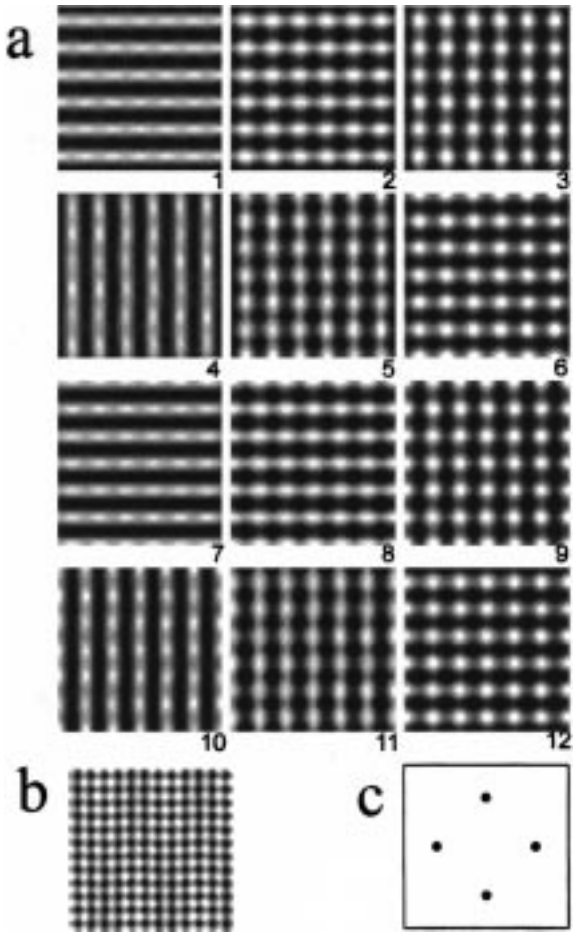

Figure 3. Square pattern in 20×20 system, $m = 28.5$ ($\epsilon = 2.4 \times 10^{-3}$): (a) snapshots of x (adjacent images are one-twelfth period apart); (b) amplitude of x oscillations showing positions of nodes (black domains) and antinodes (white domains) of standing waves; (c) two-dimensional Fourier spectrum calculated from the amplitude of x oscillations.

IV. Results

In this work we investigate a small neighborhood of the wave bifurcation with degree of supercriticality $\epsilon \leq 0.02$. Figure 1 shows dispersion curves (real part α of the complex eigenvalues vs wavenumber k) for three values of m used in our numerical experiments. The maximum value α occurs at the wavenumber k_{max}, which defines the intrinsic wavelength. For $m = 28.53$, 28.50, and 28.00, the degrees of supercriticality are $\epsilon = 0.0014$,

TABLE 1: Relative Occurrency of SW Patterns (%)

		pattern					
size	ϵ	*a*	*b*	*c*	*d*	*e*	fig
20 × 20	0.0025	55	25	15			*[a]
20 × 20	0.01	25	20	20	15	10	5
40 × 40	0.0025	35	15	15	10	10	6
40 × 40	0.01	55	20	15	10		7
20 × 19	0.0025	40	15	15	10		10
20 × 19	0.01	35	25	20	10		11

[a] Figure 3 shows pattern *a*, Figure 4 pattern *b*, and Figure 5 pattern *c*.

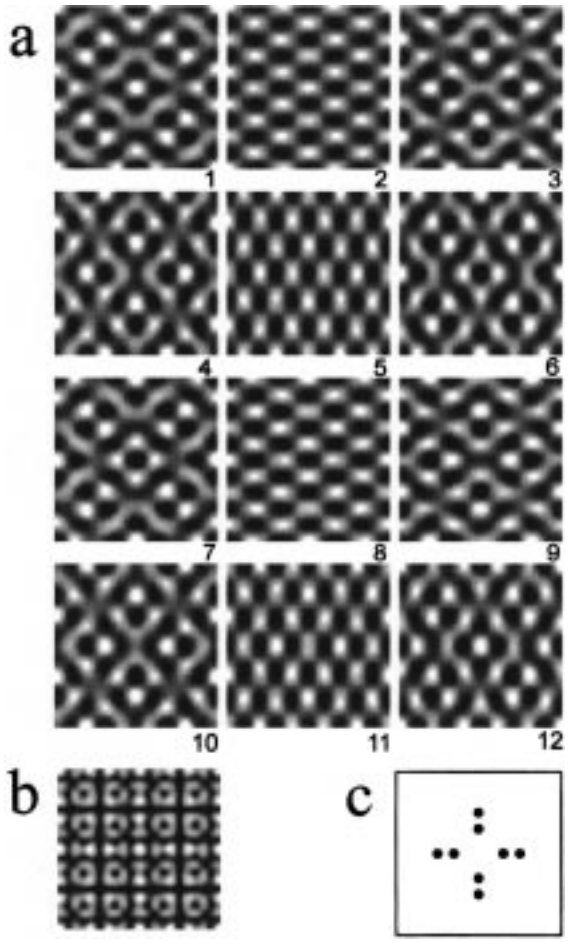

Figure 4. Rhombic pattern in 20 × 20 system, $m = 28.5$ ($\epsilon = 2.4 \times 10^{-3}$).

0.0024, and 0.02, and the intervals of k corresponding to unstable modes are 1.671−1.991, 1.616−2.042, and 1.155−2.421, respectively (see Figure 1). The period of oscillation is about 0.62 time units; this value does not change significantly in our range of supercriticality.

For brevity, we shall use here the term "stationary pattern" to refer to an established regime as opposed to a transient.

1. Transient Patterns. The transients in these simulations are often quite lengthy, especially for random IC and larger systems. For a square system of 100 × 100 space units and larger it often requires more than 20 000 time units to establish stationary patterns. For a system of 20 × 20 space units stationary patterns appeared within 5000 time units. Figure 2 shows two examples of transient patterns for a 40 × 40 square system with $m = 28.5$. Gray levels in Figure 2 correspond to the x variable, with white signifying high concentration and black low concentration. The first image in each series represents

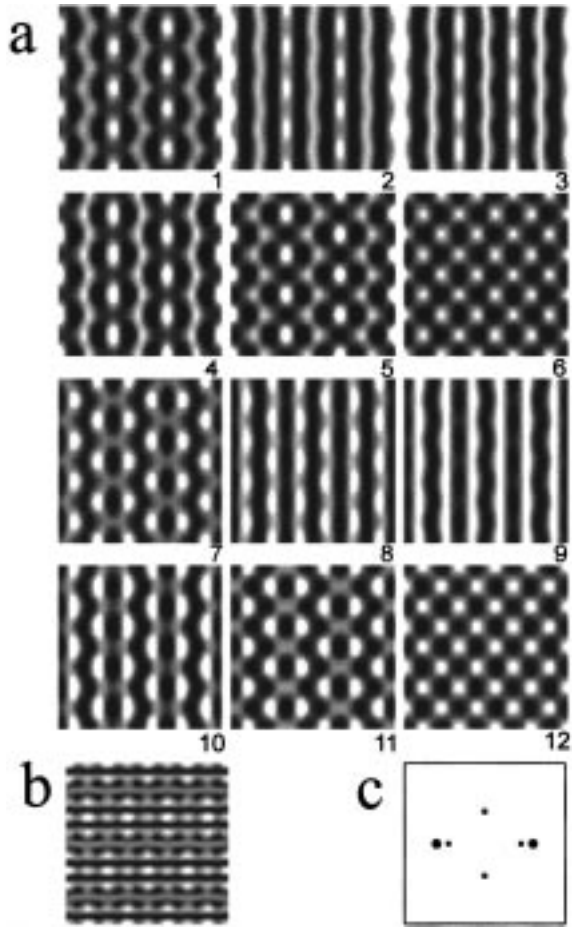

Figure 5. Stripe−rhombic pattern in 20 × 20 system, $m = 28.5$ ($\epsilon = 2.4 \times 10^{-3}$).

the initial conditions; the last image displays a snapshot of the stationary pattern. The early stages of evolution show the same type of irregular cell structure, with random elements of hexagonal and square symmetry, though the final stationary patterns are quite different in these two examples.

2. Stationary Patterns in Square Systems. To reveal the range of stationary patterns and to estimate the relative sizes of the basins of attraction for the patterns, we performed sets of 20 simulations with identical parameters and different random initial conditions. The results are summarized in Table 1.

A. Square System 20 × 20, $m = 28.5$ ($\epsilon = 2.4 \times 10^{-3}$). Figure 3a shows a cycle of oscillation of a stable square pattern. The sequence shown consists of 12 snapshots of the x-variable; adjacent images are one-twelfth of a period apart. The pattern consists of two mutually perpendicular sets of stripes that oscillate with a phase shift of $\pi/2$. Figure 3b presents the amplitude of the x-variable oscillations, thereby showing the positions of the nodes (black spots) and antinodes (white spots) of the standing waves.

Figure 3c displays the two-dimensional Fourier spectrum calculated from Figure 3b; the range on each axis is $\lambda^{-1} \in (-1, 1)$, where λ is the wavelength of the amplitude pattern. The dots indicate the locations of the major peaks in the Fourier spectra. The large dots represent Fourier peaks whose sizes are at least 75% of the largest peak; the squares signify peaks between 50% and 75% of the maximum; and small dots show peaks between 25% and 50% of the maximum. The central peak, which simply represents the spatial average, is not shown.

The Fourier spectrum in Figure 3c consists of four peaks of equal magnitude located at (±0.6, 0), and (0, ±0.6). The

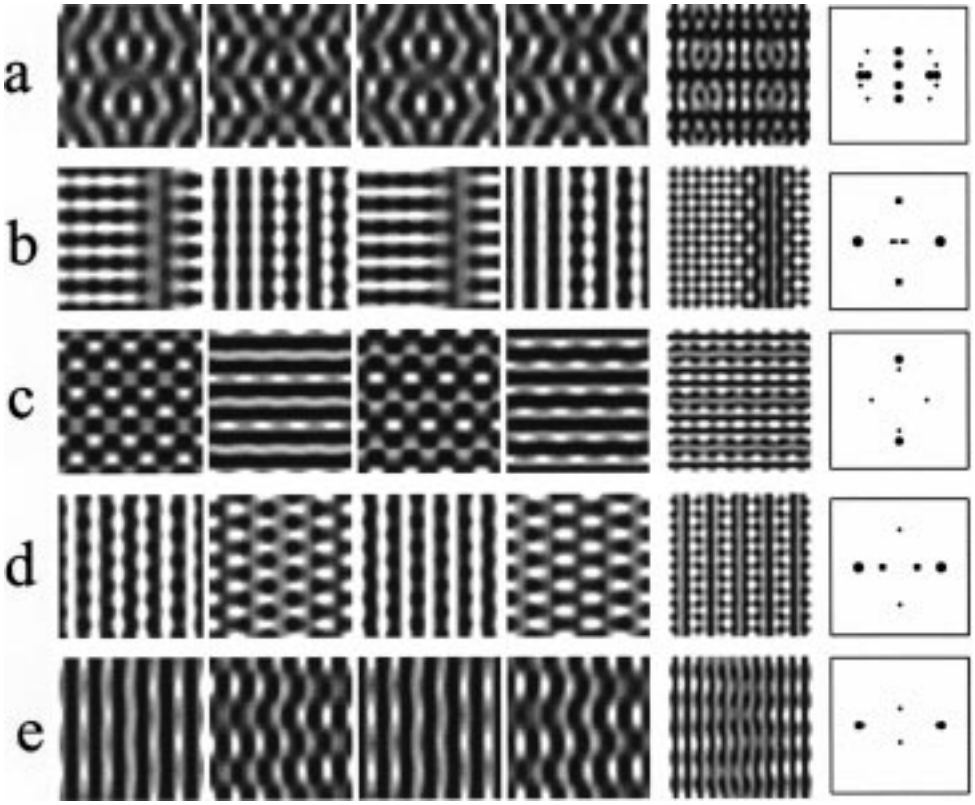

Figure 6. Standing wave patterns in 20 × 20 system, $m = 28.0$ ($\epsilon = 2 \times 10^{-2}$). First four images in each sequence display spatial patterns of x; images are one-quarter period apart. Fifth image shows amplitude of oscillations and positions of nodes and antinodes of standing waves. Last frame of each sequence depicts two-dimensional Fourier spectra calculated from amplitude x oscillations. Patterns: (a) rhombi; (b) squares with a dislocation; (c) stripes−rhombi I; (d) stripes−rhombi II; (e) modulated stripes.

corresponding wavelength of the standing wave envelope is 1.667. The wavelength of the instantaneous pattern is twice as large, i.e., $\lambda_{hor} = \lambda_{ver} = 3.333$. This wavelength is close to the intrinsic wavelength and allows exactly six wavelengths in the 20 × 20 system in each direction. The corresponding wavenumber, 1.885, lies close to the middle of the unstable domain shown in Figure 1.

The square pattern illustrated in Figure 3 emerged in 11 of the 20 simulations, which suggests that the probability for such a pattern to evolve from random IC exceeds 50%.

A different pattern, a rhombic one, is shown in Figure 4. Frames 2 and 8 display a simple rhombic pattern with $3\lambda_{hor} = L = 20$ and $5\lambda_{ver} = 20$; frames 5 and 11 show this pattern rotated by $\pi/2$. Accordingly, the Fourier spectrum in Figure 4c shows two sets of four major harmonics, which correspond to wavelengths $\lambda_1 = 6.666$ and $\lambda_2 = 4$ in both the vertical and horizontal directions. Other frames display complex rhombic patterns. This sequence of rhombic patterns occurred in 5 of our 20 simulations (see Table 1).

Figure 5 shows a pattern that emerged in 3 simulations and that can be described as an interplay of stripes and rhombi. Frames 2 and 8 display a pattern of straight stripes showing moderate amplitude modulation with $6\lambda_{hor} = 20$; frames 6 and 12 show a simple rhombic pattern with $4.5\lambda_{hor} = 20$ and $4\lambda_{ver} = 20$. The Fourier spectrum in Figure 5c contains the major harmonics with corresponding peaks at (±0.6, 0), (±0.45, 0), and (0, ±0.4).

B. Square System 20 × 20, $m = 28.0$ ($\epsilon = 2 \times 10^{-2}$). Figure 6 shows typical patterns for a larger degree of supercriticality. Each spatio-temporal pattern is displayed with six images. The first four columns portray a sequence of four spatial patterns of the x value; adjacent images are one-quarter period apart. The fifth column shows the amplitude of the x-oscillations and the positions of the nodes and antinodes of the standing waves. The two-dimensional Fourier spectra are depicted in the last frame. The patterns are presented in order of the frequency of their occurrence, with the top row containing the most frequently found pattern; the same mode of presentation is used in Figures 7−9 as well.

With increasing degree of supercriticality, the patterns become less symmetric. In Figures 3 and 4 the Fourier spectra have C_4 symmetry, and Figure 5 shows C_2 symmetry; in Figure 6 all patterns have Fourier spectra with C_2 symmetry. Comparison of Figures 6a and 4b shows the distortion of the rhombic pattern with increasing degree of supercriticality. The regular square pattern of Figure 3 emerges only rarely at the higher degree of supercriticality, and in most cases one can see a dislocation in the pattern (Figure 6b). This dislocation is caused by a phase shift of a half period between the left- and rightmost parts of the pattern. This same type of square pattern with a dislocation is seen with its transients in Figure 2. The boundary between the phase-shifted domains is always a narrow stripe-shaped domain.

All patterns shown in Figure 6c−e display stripes with a wavelength of 3.333 space units at some phase in their cycle. During most of the cycle, however, the patterns differ significantly, as can be seen in the sequences of consecutive frames and in the amplitude patterns. It is evident that with the increasing degree of supercriticality the probability of appearance of simple symmetric patterns diminishes, while less symmetric patterns emerge more often.

C. Square System 40 × 40. We repeated the above numerical experiments in a system of double the length at both values of the degree of supercriticality. Figure 7 displays the patterns

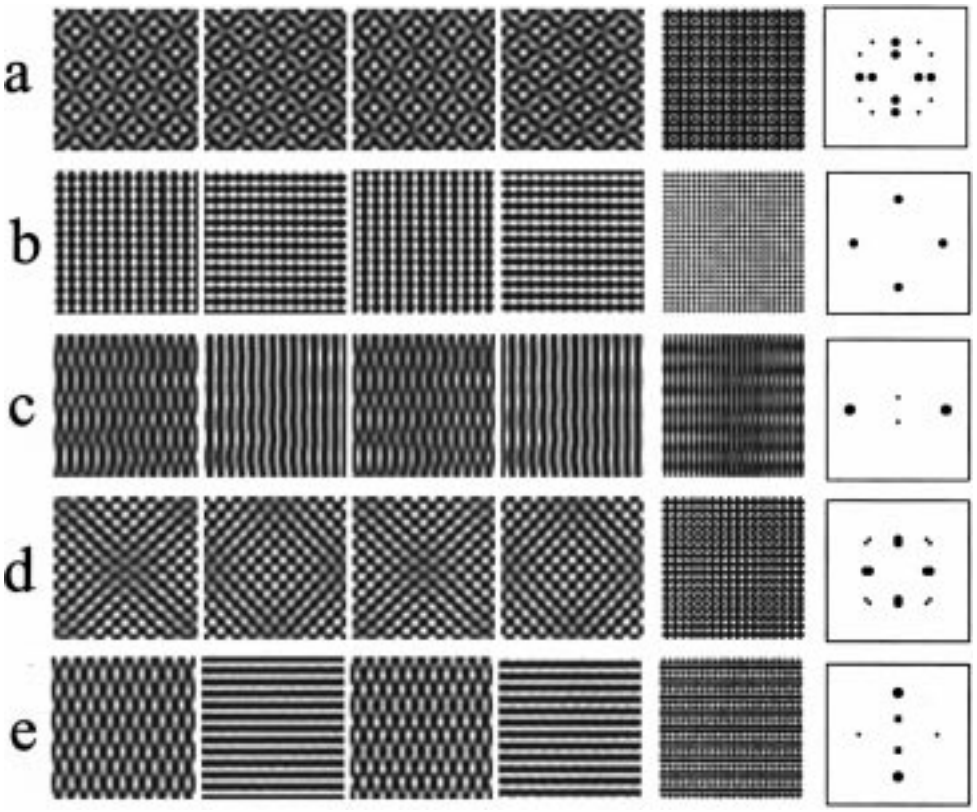

Figure 7. Standing waves in 40 × 40 system, $m = 28.5$ ($\epsilon = 2.4 \times 10^{-3}$). Patterns: (a) rhombi I; (b) squares; (c) modulated stripes; (d) rhombi II; (e) stripes-rhombi.

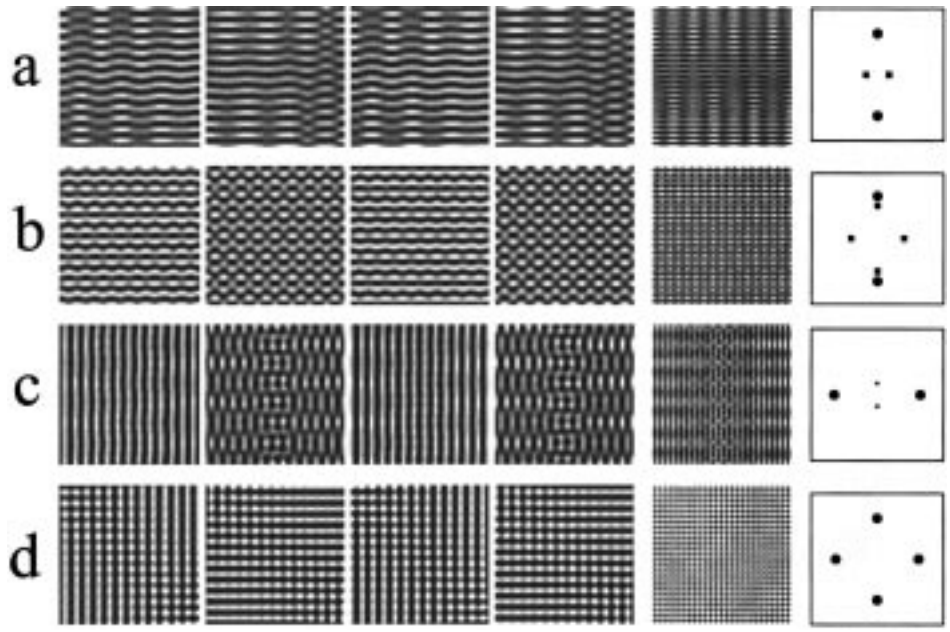

Figure 8. Standing waves in 40 × 40 system, $m = 28.0$ ($\epsilon = 2 \times 10^{-2}$). Patterns: (a) modulated stripes; (b) stripes-rhombi; (c) modulated stripes with a dislocation; (d) squares.

obtained for $m = 28.5$ ($\epsilon = 2.4 \times 10^{-3}$). The most commonly found pattern for low degree of supercriticality is the rhombic pattern (Figure 7a). The square pattern is not as frequent for the larger as for the smaller system. As we see in Table 1, the ratio of occurrences of the square and rhombic patterns is roughly 2:1 in the smaller system and 1:2 in the larger one. The pattern in Figure 7c represents modulated stripes; this pattern was not obtained in the smaller system. The pattern in Figure 7d is another variant of the rhombic pattern, while Figure 7e is the pattern that resembles that shown in Figure 6d.

Figure 8 displays the patterns found for $m = 28.0$ ($\epsilon = 2 \times 10^{-2}$). The most typical patterns here are modulated stripes, observed in 11 cases out of 20. Again, there is a relatively low probability for the square pattern to develop from random IC in this larger system. It takes a very long time to synchronize the entire pattern. Figure 8d shows the square pattern, which is still not stationary after 20 000 time units. The amplitude frame shows the pattern clearly, but it does not contain any information about phases at different locations. The snapshots of the x variable in Figure 8d show the phase shift across the system.

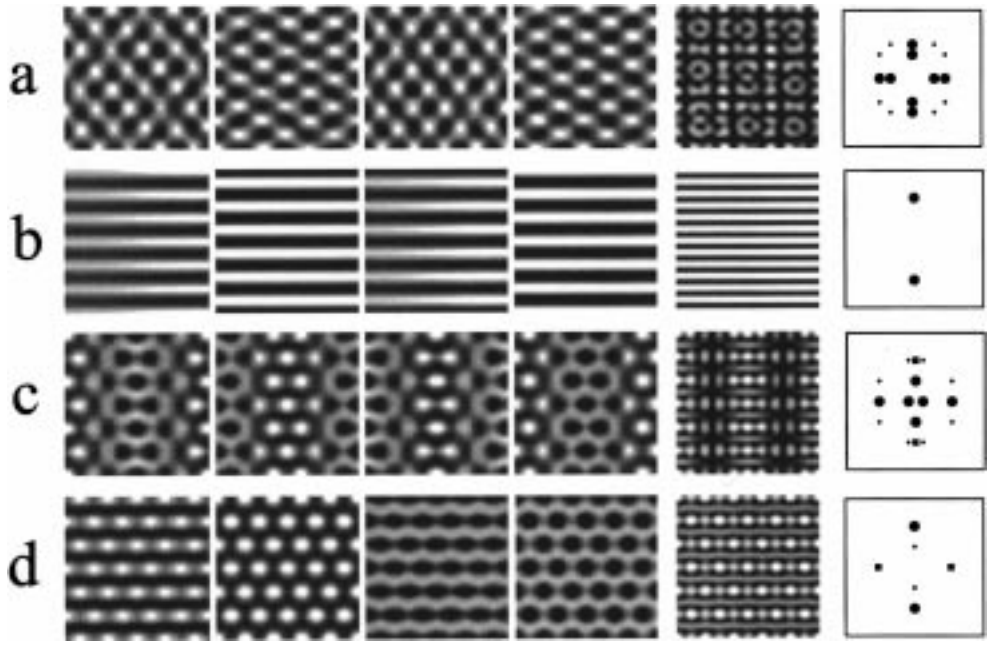

Figure 9. Standing waves in 20 × 19 system, $m = 28.5$ ($\epsilon = 2.4 \times 10^{-3}$). The vertical axis of each frame is the longer side of the rectangle. Patterns: (a) rhombi; (b) simple stripes; (c) stripes−rhombi−hexagons with two dislocations; (d) stripes−rhombi−hexagons.

Continuation of the simulations eventually leads to a pattern identical to that of Figure 7b.

3. Patterns in Rectangular Systems. The patterns found in square systems illustrate that the dominant patterns are squares, rhombi, and modulated stripes. Even in relatively large square systems (up to 200 × 200 at $m = 28.5$), we were unable to obtain standing waves consisting of unmodulated stripe patterns or hexagonal patterns. One plausible explanation is that our no flux boundaries produce an excessive perturbation to the, presumably sensitive, hexagonal structure. To check this hypothesis, we performed another set of simulations with rectangular systems, whose boundaries corresponded to the zero flux lines of hexagonal patterns. Thus the sizes were taken close to $N\lambda_i/2 \times M\lambda_i\sqrt{3}/4$, where λ_i is the intrinsic wavelength. In one set of simulations this condition was satisfied only approximately, while in the second it was fulfilled quite closely.

A. Rectangular System 20 × 19. Figure 9 shows typical stationary patterns for low degrees of supercriticality ($m = 28.5$). The vertical axis of each frame is the longer side of the rectangle. The most common pattern found here is a rhombic pattern, like that seen in square systems. The other three patterns, however, are seen only in rectangular systems. These include unmodulated stripes (Figure 9b) and hexagon−stripe patterns (Figures 9c,d).

Some of the snapshots in Figure 9d show simple hexagonal patterns. However, the spatio-temporal pattern is dominated by horizontal stripes, which appear in the Fourier spectrum as the major peaks corresponding to $\lambda_{ver} = 3.333$; the second largest pair of peaks, at $\lambda_{hor} = 3.8$, belongs to the hexagonal structure, which also modulates the amplitude of the stripes. Figure 10 presents the stable oscillatory cycle of this pattern in more detail. The cycle runs through simple stripes to modulated ones, then to rhombi, hexagons, rhombi, and then inverted hexagons (honeycomb), rhombi, modulated stripes and simple stripes.

The pattern in Figure 9c is a hexagon-stripe pattern with two dislocations. The oscillations in the middle part of this pattern are shifted by half a period from those at the sides. This behavior is analogous to that of the square pattern with a dislocation shown in Figure 6b.

Figure 11 shows patterns for the same rectangular system but with a higher degree of supercriticality ($m = 28.0$). As in the case of square systems, the higher degree of supercriticality leads to instability of the more symmetric patterns, resulting, in a majority of cases, in combinations of stripes and rhombic patterns (Figure 11a) or modulated stripes (Figure 11b). Stripe−hexagonal patterns are also found in several cases, as shown in Figure 11c. The pattern in Figure 11d is a combination of stripes and squares. We have not obtained simple stripes, squares, rhombi, or hexagons at this higher degree of supercriticality.

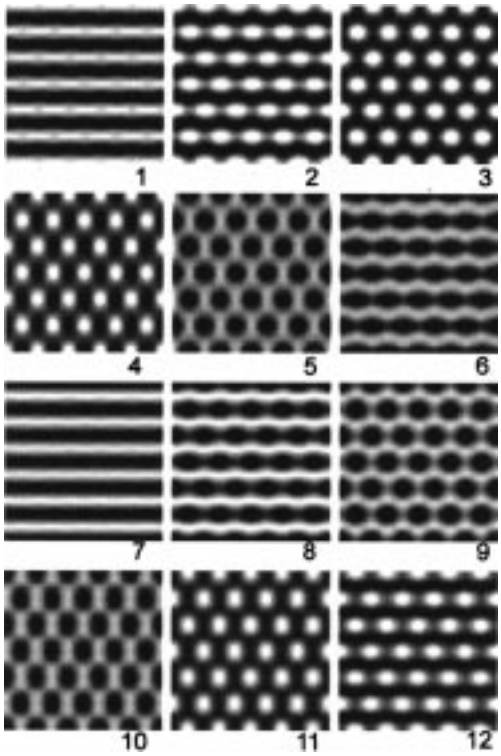

Figure 10. Stripes−rhombi−hexagons pattern in 20 × 19 system, $m = 28.5$ ($\epsilon = 2.4 \times 10^{-3}$).

B. Rectangular System 41.112 × 41.538. In terms of the intrinsic wavelength λ_i, the size of this system can be represented as $12\lambda_i \times 14\lambda_i \sin(\pi/3)$, a choice designed to minimize the perturbing effects of the no flux boundary conditions on a

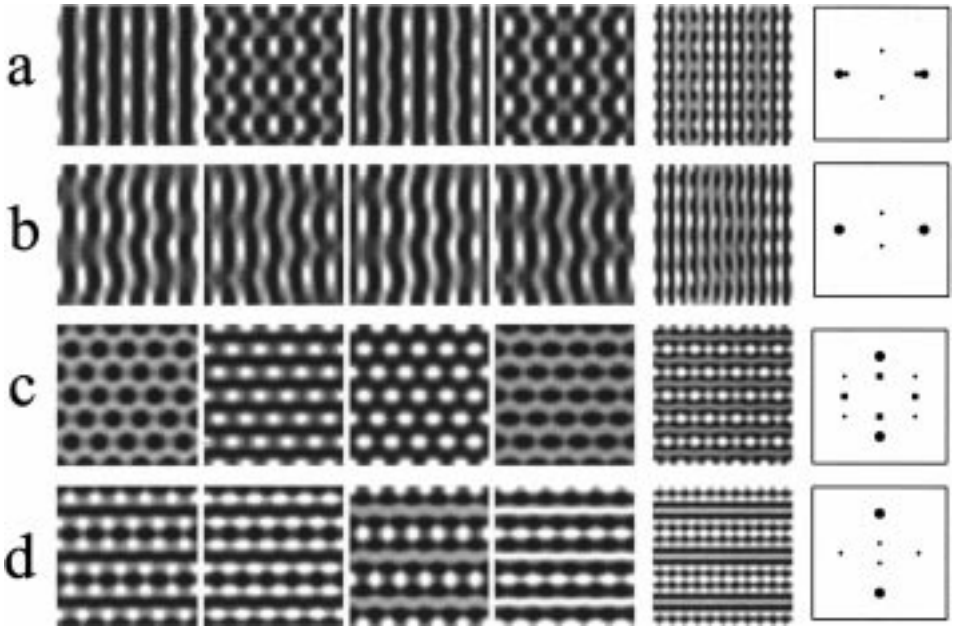

Figure 11. Standing waves in 20 × 19 system, $m = 28.0$ ($\epsilon = 2 \times 10^{-2}$). Patterns: (a) stripes−rhombi; (b) modulated stripes; (c) stripes−rhombi−hexagons; (d) stripes−squares.

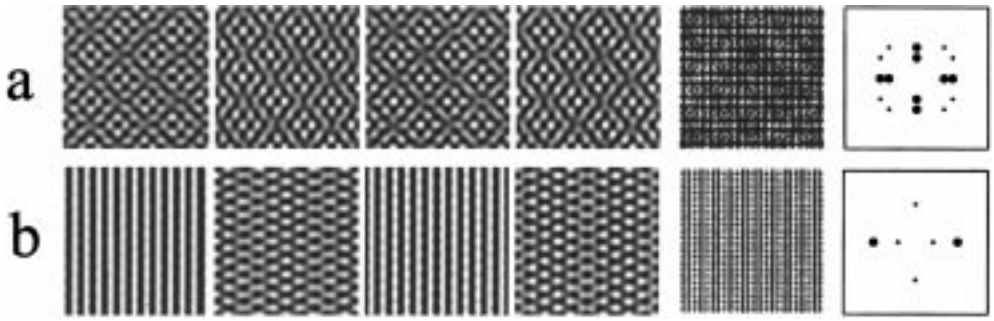

Figure 12. Patterns near the onset of short-wave instability, $m = 28.53$ ($\epsilon = 1.4 \times 10^{-3}$) in 41.112 × 41.538 system: (a) rhombi evolving from random initial conditions; (b) stripes−rhombi−hexagons evolving from hexagonal initial conditions.

hexagonal structure. Figure 12 shows two runs for $m = 28.53$ (degree of supercriticality $\epsilon = 0.0014$). The rhombic pattern shown in Figure 12a evolved from random initial conditions.

The second run was started from a superposition of three sinusoidal waves whose wave vectors formed an equilateral triangle, i.e., a perfectly fitted hexagonal structure, with one of the wave vectors perpendicular to the longer side of the rectangle. In this latter case, the orientation of the wave vectors of the pattern remained unchanged for about 3000 time units. However, the original hexagonal structure gradually evolved into two systems of plane waves whose oscillation phases were shifted by $\pi/2$. The first system appeared as a set of stripes with $12\lambda_{hor} = L_{hor} = 41.112$, aligned along the longer boundary; the second system formed a rhombic pattern. Eventually, the evolution resulted in the stationary pattern shown in Figure 12b.

At one stage of the cycle, when one system of stripes was vanishing and the other emerging, their superposition formed hexagons. The entire sequence was as follows: stripes (S1) → hexagons → rhombi → hexagons → stripes (S2). The system of stripes S2 was shifted half a spatial period with respect to the system S1. These oscillations persisted unchanged from $t \approx 12\,000$ to the end of the run at $t \approx 20\,000$ time units.

4. Stationary Patterns in Circular Systems. In search of simple hexagonal structures, we also performed simulations for a system with circular geometry, which, presumably, should favor hexagons. We found both spatially regular and irregular patterns.

We performed two sets of 10 simulations with $m = 28.5$ ($\epsilon = 2.4 \times 10^{-3}$) and different random initial conditions: one set for a system of radius $R = 10.0$ space units and a second with $R = 10.278 = 3\lambda_i$. The results are shown in Figure 13.

In the circular geometry, the symmetry of the patterns depends strongly on the degree of supercriticality. For $m = 28.5$ ($\epsilon = 2.4 \times 10^{-3}$), most patterns possess rotational symmetry. In almost all the cases the symmetry was a multiple of 3 (e.g., hexagonal patterns), as illustrated by Figure 13. In Figure 13c, however, the C_9 symmetry pattern occupying the major part of the system coexists with the C_4 pattern in the center. When the size of the system is not a precise multiple of the intrinsic wavelength λ_i, the periphery of the domain lacks rotational symmetry while the bulk of the system possesses it (Figure 13a,b).

For the higher degree of supercriticality, $m = 28.0$ ($\epsilon = 2 \times 10^{-2}$), even with the matched size of the system ($R = 3\lambda_i$), we were unable to obtain regular patterns. We have obtained time-periodic sequences of irregular patterns consisting of spots and stripes. These patterns remained spatially irregular as long as the simulations proceeded (up to 50 000 time units).

V. Discussion

We have shown previously that standing waves are the only stable patterns that emerge from the short wave instability at low degrees of supercriticality and zero flux boundary conditions

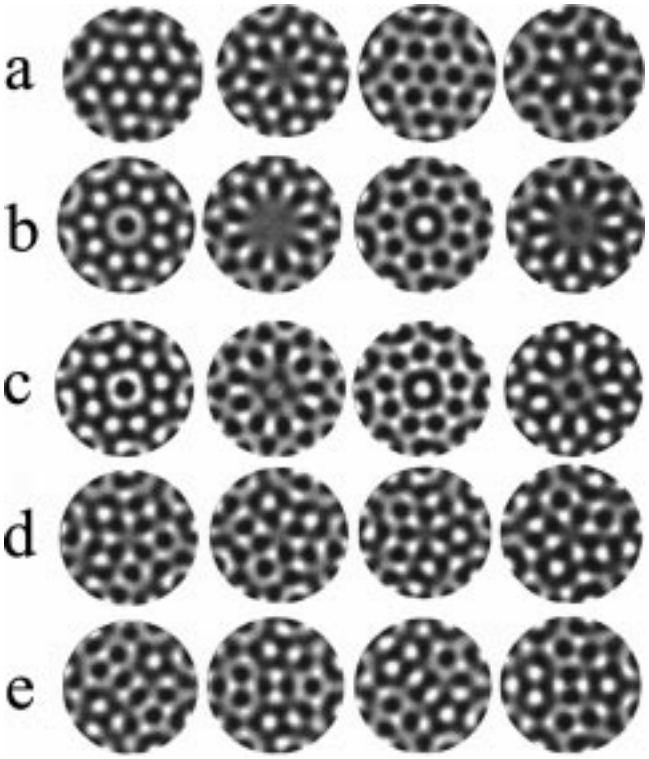

Figure 13. Standing wave patterns in circular systems, $m = 28.5$ ($\epsilon = 2.4 \times 10^{-3}$). Typical patterns for radius $R = 10$ (a, b) and $R = 10.278$ (or $R = 3\lambda_i$) space units (c−e). (a) Pattern with C_6 symmetry. (b) Pattern with C_9 symmetry. Only central parts of the patterns in (a) and (b) possess rotational symmetry; the peripheries do not. (c) Pattern with C_9 symmetry in the matched system. The whole pattern possesses rotational symmetry. (d) Pattern with a C_4-symmetric central part. (e) Pattern with a C_2-symmetric central part.

in one-dimensional systems.[3] Here we have investigated what types of standing waves occur in two-dimensional systems at low degrees of supercriticality. We have found simple and modulated stripes, squares, and rhombi. We have also seen cycles that oscillate between instantaneous stripes and rhombic patterns, and patterns consisting of sequences of stripes, rhombi, and hexagons.

We were unable to obtain simple hexagonal patterns in matched rectangular systems, even when we started from initial conditions very close to the expected pattern. This finding stands in contrast to results for two-dimensional patterns arising from the aperiodic Turing instability in reaction−diffusion systems. In the latter case, the basic patterns are hexagons and stripes, while stable squares or rhombi have not been found.[2,9]

On the other hand, the single oscillatory cycle shown in Figure 10 displays all the basic patterns related to the aperiodic Turing instability: stripes, hexagons, and inverted hexagons (honeycomb), as well as rhombi and modulated stripes. It seems likely that the short-wave instability can give rise to an even greater variety of spatio-temporal patterns than the aperiodic Turing and the long-wave oscillatory instabilities.

With random initial conditions, the frequency of occurrence of various patterns should be proportional to relative areas of their basins of attraction. In our simulations, in square systems of smaller size at a low degree of supercriticality, the dominant pattern is squares. As the degree of supercriticality and/or the system size is increased, rhombic patterns become dominant, and then modulated stripes occur most frequently. We note also that we find a significant number of stable patterns that contain defects or dislocations due to phase shifts between oscillations in neighboring regions. Some of the patterns presented in this paper have been studied earlier by Dionne et al. from the point of view of their symmetry without considering their stability.[10]

In circular systems we find regular patterns with elements of C_6, C_9, and C_4 symmetry. All regular patterns consist of spots; we have not found regular patterns containing stripe elements.

This paper presents only the first step in the study of standing wave patterns in two-dimensional systems. The most crucial test of the significance of our results lies in the experimental search for the fascinating patterns that these simulations have generated. We hope that modifications of the BZ and CIMA/CDIMA chemical oscillators, which have yielded the majority of known chemical patterns,[11] will result in emergence of the short-wave instability and the corresponding patterns. One can estimate the expected scale of such patterns. The characteristic wavelength of the patterns in our model is 3.43, and the period of oscillations is about 0.62. The typical period of oscillation in liquid-phase reactions is about 1 min. The scaling in eq 2 then gives the characteristic wavelength of the expected patterns as about 1 mm.

Acknowledgment. We gratefully acknowledge the support of the National Science Foundation Chemistry Division and the W. M. Keck Foundation.

References and Notes

(1) Turing, A. M. *Philos. Trans. R. Soc. London* **1952**, *B237*, 37.
(2) Cross, M. C.; Hohenberg, P. C. *Rev. Mod. Phys.* **1993**, *65*, 851.
(3) Zhabotinsky, A. M.; Dolnik, M.; Epstein, I. R. *J. Chem. Phys.* **1995**, *103*, 10306.
(4) Dolnik, M.; Zhabotinsky, A. M.; Epstein, I. R. *J. Phys. Chem.* **1996**, *100*, 6604.
(5) Dolnik, M.; Zhabotinsky, A. M.; Epstein, I. R. *J. Chem. Soc., Faraday Trans.* **1996**, 92, 2919.
(6) Gray, P.; Scott, S. K. *Chemical Oscillations and Instabilities*; Clarendon, Oxford, U.K., 1990.
(7) Hindmarsh, A. C. In *Scientific Computing;* Stepleman, R. S., et al., Eds.; North-Holland: Amsterdam, 1983; p 55.
(8) Press: W. H.; Flannery, B. P.; Teukolsky, S. A.; Vetterling, W. T. *Numerical Recipes*; Cambridge University Press: Cambridge, U.K., 1986.
(9) Borckmans, P.; Dewel, G.; De Witt A.; Walgraef, D. In *Chemical Waves and Patterns*; Kapral, R., Showalter, K., Eds.; Kluwer: Dordrecht, The Netherlands, 1995; p 323.
(10) Dionne, B.; Golubitsky, M.; Silber, M.; Stewart, I. *Philos. Trans. R. Soc. London*, **1995**, *A352*, 123.
(11) Kapral, R.; Showalter, K., Eds. *Chemical Waves and Pattern*; Kluwer: Dordrecht, The Netherlands, 1995.